

Optimal interdigitated electrode sensor design for biosensors using multi-objective particle-swarm optimization

Issa Sabiri¹, Hamid Bouygh², Abdelhadi Raihani¹

¹EEIS Laboratory, ENSET Mohammedia, Hassan II University of Casablanca, Casablanca, Morocco

²LSIB Laboratory, Faculty of Sciences and Techniques, Hassan II University of Casablanca, Casablanca, Morocco

Article Info

Article history:

Received Jul 5, 2022

Revised Aug 22, 2022

Accepted Sep 2, 2022

Keywords:

Impedance spectroscopy

Interdigitated electrodes

Optimization

Particle swarm optimization algorithm

Sensitivity

ABSTRACT

Interdigitated electrodes (IDEs) are commonly employed in biological cellular characterization techniques such as electrical cell-substrate impedance sensing (ECIS). Because of its simple production technique and low cost, interdigitated electrode sensor design is critical for practical impedance spectroscopy in the medical and pharmaceutical domains. The equivalent circuit of an IDE was modeled in this paper, it consisted of three primary components: double layer capacitance, C_{dl} , solution capacitance, C_{Sol} , and solution resistance, R_{Sol} . One of the challenging optimization challenges is the geometric optimization of the interdigital electrode structure of a sensor. We employ metaheuristic techniques to identify the best answer to problems of this kind. multi-objective optimization of the IDE using multi-objective particle swarm optimization (MOPSO) was achieved to maximize the sensitivity of the electrode and minimize the Cut-off frequency. The optimal geometrical parameters determined during optimization are used to build the electrical equivalent circuit. The amplitude and phase of the impedance versus frequency analysis were calculated using EC-LAB® software, and the corresponding conductivity was determined.

This is an open access article under the [CC BY-SA](https://creativecommons.org/licenses/by-sa/4.0/) license.



Corresponding Author:

Issa Sabiri

EEIS Laboratory, ENSET Mohammedia, Hassan II University of Casablanca

Casablanca, Morocco

Email: issa.sabiri@etu.fstm.ac.ma

1. INTRODUCTION

Giaever and Keese created the key impedance-based technology known as electrical cell-substrate impedance sensing (ECIS) in 1984 for the in-vitro, real-time evaluation of biological cellular activities [1]. Traditional round gold electrodes were employed to research cell adhesion, proliferation, migration, invasion, and barrier activities in the early stages of biosensor development [2]–[6]. Non-ionizing radiation interactions with biological matter are progressing in diagnostic and therapeutic issues. The electromagnetic properties of the propagation medium must be determined in order to make progress [7]. Another application aspect that requires the values of electrical characteristics such as conductivity and permittivity of biological tissues is public health problems related to electromagnetic fields (dosimetry, biological impacts). These biological tissue values at the frequencies of interest are unknown [8].

The electrode design has a significant impact on biosensor accuracy and sensitivity. Cell-based biosensors offer a wide range of applications, including clinical diagnostics, drug discovery, and electrophysiology

[9]. Impedimetric and conductometric approaches can be used to measure morphological changes in cells, which are impacted by the electrode geometry [10]–[11]. Microelectrodes have several advantages over conventional macroscopic electrodes, including cost, high current densities during measurement, and the ability to integrate them into other instrumental devices to create portable measurement systems, or even biochips or lab-on-chips.

Microelectrodes, on the other hand, have a substantially larger resistance than macroelectrodes due to contact phenomena. The interaction between ions and molecules at the border between the electrolyte's surface and the measuring electrodes causes an interface capacitance, or double layer, which manifests these phenomena. This capacitance is inversely proportional to the surface area of the electrodes. As a result, the double layer capacitance acts as a limitation, increasing measurement inaccuracy.

In all engineering fields, particularly in electronics used in biomedical circuits, reliable, efficient, and robust optimization strategies are highly desired [12]. In this paper, we emphasize the application of a bio-inspired technique, specifically particle swarm optimization. The optimization of IDEs or sensor shape is critical since it can enhance the bioimpedance measurement range, allowing for the most accurate cellular electrical depiction. Several methods for optimizing interdigitated electrodes (IDEs) for bioimpedance spectroscopy have already been investigated. Ibrahim *et al.* [13] used analytical modeling and simulation to investigate the relationship between design factors and IDE frequency behavior in order to optimize configuration for a square area cross section. Zhang *et al.* [14] used mathematical models to investigate the effect of electrode size on ECIS sensitivity. Ngo *et al.* [15] used a modeling and experimental technique to optimize geometrical parameters for biological media characterisation by reducing polarization impact and Mansor and Nordin [1] examine the distribution of electric fields on various sensor geometries. Some research, such as the optimization of IDEs for HS578T cancer cells [11], are more application specific. However, there hasn't been much research into employing metaheuristics algorithms to improve the IDE's sensitivity and cut-off frequency (F_{Low}). For cellular research, the shape of the sensor can be changed to get more sensitive and accurate results.

This research shows the similar circuit model of IDEs that are optimized for blood abnormalities. The ECIS technique is used to optimize the IDEs' design to increase sensitivity to changes in blood cells. The ECIS approach enables accurate electrical representation of a cell's biological response. Using the multi-objective optimization approach based on the particle swarm optimization (PSO) algorithm, the IDE's shape will be adjusted so that the IDE's sensitivity is maximized and the cut-off frequency of the interfacial impedance is minimized. The corresponding circuit model is analytically modeled in section 2. Section 3 looks into multi-objective optimization using PSO and the methodology to introduce the objective function from two different perspectives: sensitivity and cut-off frequency. The optimization results and conclusion are presented in section 4.

2. THEORETICAL BACKGROUND

2.1. Biosensors with interdigitated electrodes

Single-plane electrodes are used in biosensors with interdigitated electrodes, which are manufactured via traditional metal deposition [16]. Sensors with interdigital electrodes have been designed to identify deoxyribonucleic acid (DNA) sequences using impedance spectroscopy and blood analysis, and have been improved to improve the frequency band. An interdigital sensor, as illustrated in Figure 1, is made up of two comb-shaped metal electrodes, each with a width W , a length L of electrodes, and a spacing S between two consecutive electrodes.

An interdigital electrode sensor works on the same concept as a parallel plate capacitor. The sensor is deposited on a substrate, and a voltage is used to create an electric field between the two electrodes. An electromagnetic field is created and travels through the sensor when a biological component is placed on it [10]. The geometry of the object under research and the biological fluid's dielectric characteristics affect the capacitance and conductance between the two electrodes. Depending on the use, the difference in the electric fields is used to describe how the biological environment affects the organism. Based on the equivalent circuit, the total impedance can be represented as (1).

$$Z = 2.Z_{dl} + Z_{Rsol} // Z_{Csol} = \frac{2}{j\omega C_{dl}} + \frac{R_{sol}}{(1 + j\omega C_{sol} \cdot R_{sol})} \quad (1)$$

The impedance modulus R_{sol} or resistance of the electrolyte solution mimics the conductive effects of the

medium under the influence of an electric field. This is the measurement's most delicate component. To mathematically explain the effect of the IDE geometry on each component of the equivalent circuit model, Olthuis *et al.* [17] created a new parameter called the cell constant, K_{Cell} . The proportionality factor between the electrolyte's resistivity/permittivity and the actual measurement is K_{Cell} , which only exists at the electrode-electrolyte interface. It is fully dependent on the sensor's geometry, as illustrated in (2)-(5).

$$R_{sol} = \frac{K_{Cell}}{\sigma_{Sol}} \quad (2)$$

With:

$$K_{Cell} = \frac{2}{(N-1)L} * \frac{\Gamma(k)}{\Gamma\sqrt{1-k}} \quad (3)$$

$$\Gamma(K) = \int_0^1 \frac{1}{\sqrt{(1-t)(1-kt)}} \quad (4)$$

$$K = \cos\left(\frac{\pi}{2} * \frac{W}{W+S}\right) \quad (5)$$

The dielectric component of the material under test is represented by C_{cell} . It depicts the two electrodes' direct capacitive interaction. The dielectric permittivity is proportional to the capacitance.

$$C_{Cell} = \frac{\epsilon_0 \epsilon_r Sol}{K_{Cell}} \quad (6)$$

The impedances that describe the interface effects produced at the electrode-electrolyte interfaces are made possible by the double-layer capacitance C_{dl} . Both the electrolyte solution and the material used to form the electrodes have an impact on the impedances. The simple capacitive coupling between the two electrodes is what is meant by the capacitance that mimics the dielectric portion of the medium under test. The dielectric permittivity and this capacitance are connected by (7).

$$C_{dl} = 0,5 * A * C_{(dl, Surface)} = 0,5 * W * L * N * C_{(dl, Surface)} \quad (7)$$

The overall electrode surface area is A. When a factor of 0.5 is applied, a single capacitance C_{dl} is produced by dividing in half the two interface capacitances produced by interface effects at the entire electrode surface. In the case of interdigitated electrodes, this surface equals the electrode length times their width times the number of electrodes. The characteristic double layer called Stern's capacity, $C_0 = 0.047F/m^2$, for electrolytes with a very high ionic concentration is thought to be the same as the characteristic double layer capacity, C_{dl} , surface.

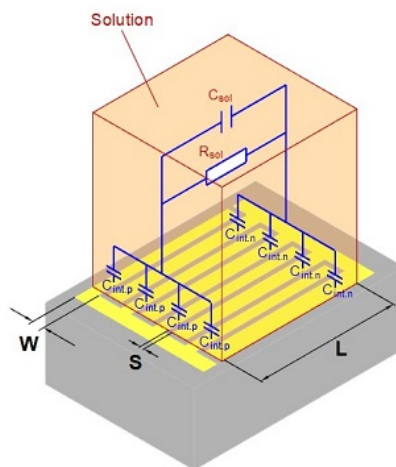


Figure 1. Similar circuit model of IDEs in a liquid environment

2.2. The IDE's sensitivity

Bouyghf *et al.* [12] and Mansor *et al.* [1] have shown that two cut-off frequencies separate the dominance of components, namely F_{Low} and F_{High} . The Z_{Sol} will be quite high at frequencies between F_{Low} and F_{High} , and the C_{Sol} will behave practically as an open circuit, allowing current to flow through the C_{dl} and R_{Sol} branches. C_{dl} prevails at lower frequencies below F_{Low} , about a few kHz. F_{Low} frequencies ranging from 0 to hundreds of kHz are dominated by R_{Sol} .

With increasing frequency, the impedance reduces until it reaches F_{Low} . The double-layer capacity, however, does not intervene in the overall impedance above the cutoff frequency F_{Low} . Because only the resistance R_{Sol} (or modulus of total impedance) affects impedances less than F_{High} , and because C_{Cell} is not yet informative, this is the case. In this frequency band, which is limited by F_{Low} and F_{High} , the total impedance is the same no matter what frequency it is.

The observed impedance is based on the total impedance fields and represents an accurate measurement of the biological sample within this range (for example, the conductivity, which can be estimated from the R_{Sol} value). We might draw the conclusion that the sensitivity of the frequency measurement needs to be improved. The dominant impedance spectra of the R_{Sol} module's need a wider frequency range. By reducing the low cut-off frequency F_{Low} as much as is practical, increasing the frequency range (also referred to as the useful frequency range) prevents the interface phenomenon represented by the double layer capacitance. In square structure of IDEs with an LxL dimension, (8) and (9) determine the sensitivity (Sen) and cut-off frequency F_{Low} respectively.

$$Sen = \frac{\Delta Z}{\Delta \sigma} = \frac{(|Z_2| - |Z_1|)}{(\sigma_2 - \sigma_1)} \quad (8)$$

$$F_{Low} = \frac{\sigma_{sol}}{\pi K_{Cell} C_{dl}} \quad (9)$$

3. METHOD

3.1. Multi-objective optimization

The following is a mathematical formulation of the general multi-objective optimization problem: minimize

$$H(\vec{x}) = [h_1(\vec{x}), h_2(\vec{x}), \dots, f_k(\vec{x})]^T$$

subject to:

$$\begin{cases} \vec{f}(\vec{x}) \leq 0 \\ \vec{g}(\vec{x}) = 0 \end{cases}$$

$$\vec{x} \in R^n, \vec{h}(\vec{x}) \in R^k, \vec{f}(\vec{x}) \in R^m \text{ and } \vec{g}(\vec{x}) \in R^q.$$

$$X = \vec{x} \mid f_m(\vec{x}) \leq 0, m = 1, 2, 3, \dots, m, g_q(\vec{x}) = 0, q = 1, 2, 3, \dots, q, S = H(\vec{x}) \mid \vec{x} \in X$$

Here $\vec{x} \in R^n$ is the vector of design variables and n is the number of decision variables. $k \geq 2$ is the number of objective functions, and $H(\vec{x}) \in R^k$ is their vector in which $h_i(\vec{x}) : R^n \rightarrow R^1$. In addition, m and $\vec{f}(\vec{x})$ stand for the quantity and direction of inequality restrictions, respectively. The number of equality constraints and their vector, respectively, are q and $\vec{g}(\vec{x})$. The feasible decision and criteria spaces, respectively, are X and S.

Machairas *et al.* [18] proposed one of the most prominent approaches for presenting multi-objective solutions. If there is no other possible option that improves one goal without worsening at least one other, it is called a Pareto or non-dominated solution. For solving multi-objective optimization problems, there are two main types of decision-making techniques. The second searches simultaneously for all non-dominated solutions, as opposed to the first, which solves a single objective problem for each Pareto-optimal solution [19]–[21].

The most popular multi-criteria decision-making approach in decision theory is the weighted sum method (WSM) [22]. By summing standardized objective functions scaled by their weighting coefficients, ki, the weighted sum technique can reduce the multi-objective task of reducing a vector of criteria functions into such a scalar problem. In [23] shows the formula for the weighted sum method as (10):

$$H_{ws}(x) = \sum_{i=1}^k \lambda_i \frac{h_i(x) - h_i(x)^{min}}{h_i(x)^{max} - h_i(x)^{min}} \quad (10)$$

where $H_{ws}(x)$ is the overall objective function, k is the number of objective functions $h_i(x)$ and $\lambda_i \in [0, 1]$ when $\sum_{i=1}^k \lambda_i = 1$. In addition, $h_i(x)^{min}$ and $h_i(x)^{max}$ are the minimum and maximum values of the objective functions, respectively, as they are optimized independently.

3.2. Multi-objective particle swarm optimization (MOPSO)

The particle swarm optimization (PSO) algorithm was created in 1995 by Eberhart and Kennedy [24]. This stochastic optimization method is population-based. In order to determine the best solution, the PSO method first generates a set of random particles. At the conclusion of each generation, the two best values are applied to each particle. The first option has so far had the best results. Another is the highest value that any population particle has ever attained. This is the world's best value. The best value is a local best when a particle uses the population as its topological neighbors. Once you know the two best values for a particle's speed and location, you can change them [25]. The position of $x_i(t)$ is calculated by adding its velocity, $v_i(t)$ to the current position, i.e:

$$x_i(t) = x_i(t-1) + v_i(t). \quad (11)$$

where the velocity vector is expressed as (12).

$$v_i(t) = wv_i(t-1) + C_1r_1[P_{best} - x_i(t)] + C_2r_2[G_{best} - x_i(t)] \quad (12)$$

The inertia weight w is used to influence the effect of the particle's previous velocity on the current velocity. C_1 is the cognitive learning factor, which shows how interested a particle is in its own success. C_2 is the social learning factor, which shows how interested a particle is in the success of its neighbors. Positive constants, C_1 and C_2 , are commonly used [21]. Furthermore, r_1 and $r_2 \in [0, 1]$ are two independent random number sequences used to avoid entrapment on local minimums and to allow a tiny number of particles to diverge in a more thorough search of the search space [26]; the personal and global best positions are P_{best} and G_{best} . Figure 2 shows the particle swarm optimization algorithm's velocity and position updates. To turn a PSO algorithm into a MOPSO, it is common to create an external repository to store the non-dominated solutions and use a leader selection method to pick a global leader for the particles from a group of equally good solutions based on some criteria. When the external repository fills up, an archiving method is required to prune it and keep it at a predetermined size, removing non-dominant solutions based on some criterion. Due to the large number of non-dominated populations, this criterion has a big effect on the quality of the solutions found by the search, especially when there are many goals.

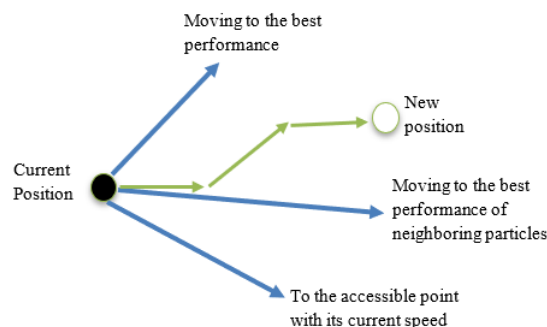


Figure 2. The updating process of the particle velocity

3.3. Formalization

The optimization problem can be incisively described as following maximize the sensibility (Sen) subject to minimize F_{Low} where:

$$S_{min} \leq S \leq S_{max}$$

$$W_{min} \leq W \leq W_{max}$$

$$N_{min} \leq N \leq N_{max}$$

Sen is given by (8) and $S_{min,max}$, $W_{min,max}$, $N_{min,max}$ is the minimum and maximum of each parameter appropriate to the IDEs. This makes it easier for the algorithm to find the best design parameters for the best performance.

To resolve multiobjective problems, we proposed the algorithm given in Figure 3. The parameter settings have been fine-tuned to provide the best possible result. As mentioned already, our IDE is optimized in order to improve the sensitivity, have reduced solution resistance, and have a low cut-off frequency. The MOPSO algorithm was utilized in this method because of its good reputation when it comes to optimizing multiple objective functions. The optimization was done considering the electrolytic medium with a change of $\Delta\sigma = \pm 0.110^{-6} S$. Global parameters and data used are shown in Table 1.

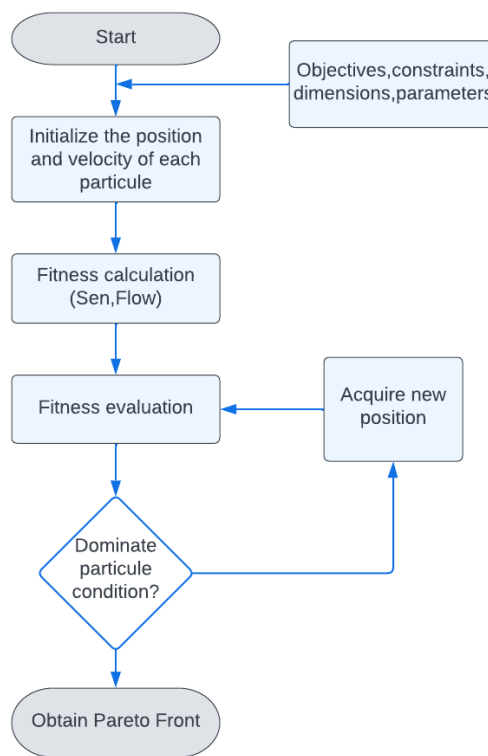


Figure 3. Flowchart for the intended simulation-based method to optimization

Table 1. Parameters and technical data

Parameter	Designation
$nPop$	Population Size (=100)
$nRep$	Repository Size (=10)
$MaxIt$	Maximum Iterations (=1000)
$alpha$	Grid Inflation Parameter (0.1)
$nGrid$	Number of Grids per each Dimension (=100)
$beta$	Leader Selection Pressure Parameter (=2)
$gamma$	Repository Member Selection Pressure (=4)
$\Delta\sigma$	Electrolytic medium change (=0.1 $10^{-6} S$)
$W_{lb} - W_{ub}$	Lower and Upper Bounds (1-100 μm)
$S_{lb} - S_{ub}$	Lower and Upper Bounds (1-100 μm)
$N_{lb} - N_{ub}$	Lower and Upper Bounds (2-100)
L X L	Square length of the IDE (6x6 mm)

4. SIMULATION RESULTS

This section was focused on discussion of the multi-objective particle swarm optimization results for the proposed application of our objective functions. We used MATLAB software to find the optimum result for each parameter. The equivalent circuit model was implemented using EC-LAB® tools to validate the theory.

4.1. Optimization result

After fixing each parameter and technical data on the MATLAB software, the number of iterations was set to 1,000 and the function tolerance was set to 10^{-4} . The best outcomes are depicted in Figure 4 and summarized in Table 2. The best-picked selected solution responds to our goals and criteria, according to Preto Front analysis. L must adhere to the linear equality that follow: $N.(W + S) \approx 6 \text{ mm}$, with a maximum sensitivity of 437.75 Ohm.m/S and a minimum cut-off frequency of 35.53 Khz.

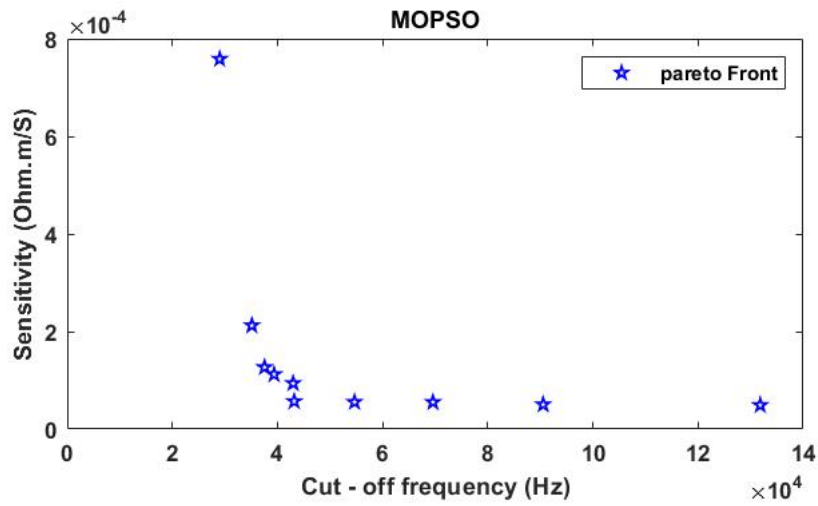


Figure 4. Pareto front

Table 2. Parameters and technical data

$W_{opt}(\mu m)$	$S_{opt}(\mu m)$	N_{opt}	$N.(S + W)(mm)$	Sensitivity (Ohm. $\mu m/S$)	$F_{Low}(Khz)$
98.04	65.01	45.30	97.40	237.19	43.45
76.52	93.17	28.35	4.81	48.74	28.15
92.91	99.00	67.35	12.92	106.53	38.09
96.00	58.82	40.33	6.24	332.72	470.93
18.08	11.00	54.11	1.57	165.68	140.34
71.77	40.08	99.00	11.07	48.10	97.88
84.97	16.58	29.25	2.97	576	194.93
cyan99.13	78.32	33.48	5.94	437.75	35.53
75.63	11.86	64.47	5.64	116.34	312.06

4.2. Electrical simulation using equivalent circuit

The optimal geometrical parameters determined during optimization are used to build the electrical equivalent circuit. The amplitude and phase of the impedance versus frequency analysis were calculated using EC-LAB® software, and the corresponding conductivity was determined. The corresponding circuit components are summarized in Table 3.

The total electrical impedance Z_{jw} can be trigonometrically expressed as in (13).

$$Z_{jw} = |Z_{jw}|e^{i\theta} \quad (13)$$

The resistance R_{sol} will be presiding from the cut-off frequency F_{Low} then the total impedance can be simplified as (14).

$$F_{Low} = \frac{R_{Sol}}{(1 + jwC_{Sol}R_{Sol})} \quad (14)$$

The conductivity can be expressed as showing in (15).

$$\sigma_{Sol} = \frac{k_{Cell}}{|Z_{jw}|} \cos(\theta) \tag{15}$$

Table 3. Equivalent circuit components

$R_{Sol} (\Omega)$	$C_{Sol} (pF)$	$C_{dl} (\mu F)$
11.82	41.73	0.76

The characteristics of the designed biosensors is essential for the effective use of impedance spectroscopy in the medical and pharmaceutical fields. The technical features of the designed IDE at the acquisition frequency Fmdl simulated under its equivalent circuit. As shown in Figure 5, Figure 6, and Table 4.

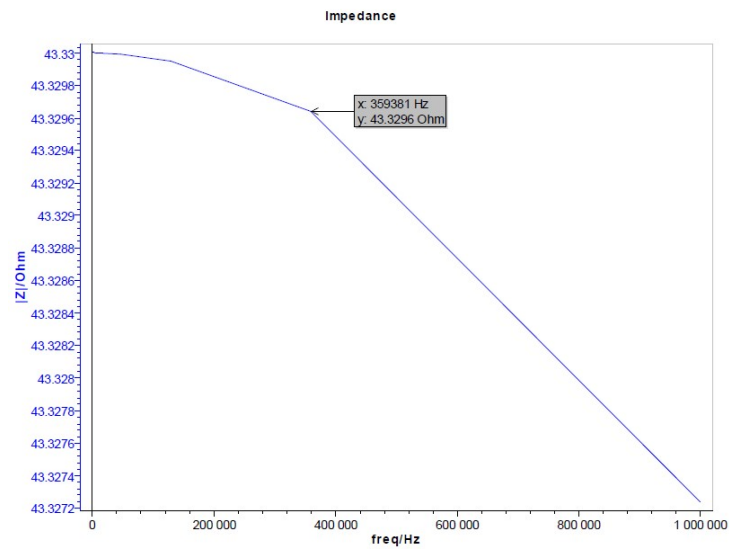


Figure 5. Impedance vs. frequency analysis using EC-LAB® software

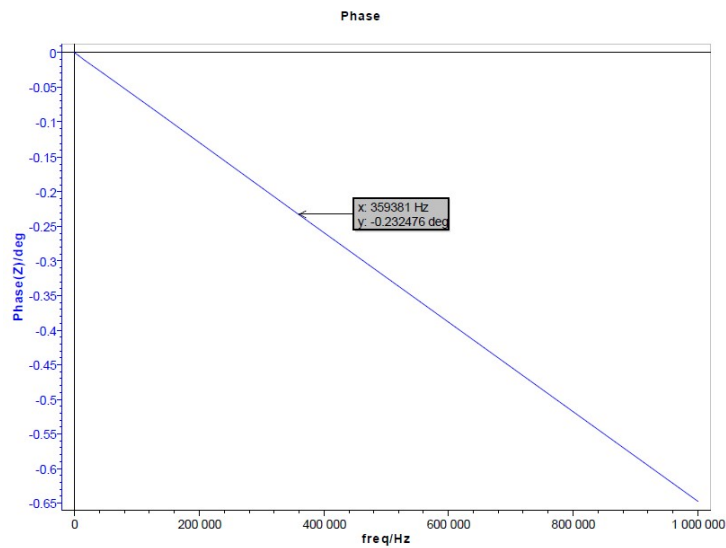


Figure 6. Phase vs. frequency analysis using EC-LAB® software

Table 4. Characteristics of the IDE

$W(\mu m)$	$S(\mu m)$	N	L (mm)	$K_{Cell}(\mu m^{-1})$	$Sen(\Omega.\mu m/S)$	$F_{midl}(MHz)$	$\sigma_{measured}(S/\mu m)$
99.13	78.32	34	6	10.41	437.75	0.36	$0.24 \cdot 10^{-6}$

5. CONCLUSION

This study presents a physical model of an IDE that uses the MOPSO algorithm and Pareto Front analysis to detect DNA sequences utilizing impedance spectroscopy and blood analysis. The simulation results demonstrate the benefit of improving the sensor's components. Finally, utilizing the best results, we built the electrical equivalent circuit components and analyzed their impedance responses with the EC-LAB® program. Theoretical and simulation results support the concept of having a maximum sensitivity and a low cut-off frequency. However, factors such as electrical field distribution, fabrication process capabilities, working area limitation, and relevance to the intended application limit the ideal configuration's selection.




REFERENCES

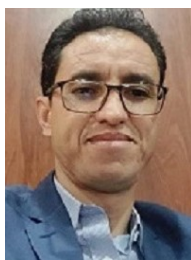
- [1] A. F. M. Mansor and A. N. Nordin, "Theoretical modelling of interdigitated electrode sensor for mammalian cell characterization," in *2018 7th International Conference on Computer and Communication Engineering (ICCCCE)*, Sep. 2018, pp. 62–67, doi: 10.1109/ICCCCE.2018.8539280.
- [2] I. Giaever and C. R. Keese, "Micromotion of mammalian cells measured electrically," in *Proceedings of the National Academy of Sciences*, Sep. 1991, pp. 7896–7900, doi: 10.1073/pnas.88.17.7896.
- [3] C. M. Lo, C. R. Keese, and I. Giaever, "Cell-substrate contact: another factor may influence transepithelial electrical resistance of cell layers cultured on permeable filters," *Experimental Cell Research*, vol. 250, no. 2, pp. 576–580, 1999, doi: 10.1006/excr.1999.4538.
- [4] C. R. Keese and I. Giaever, "Monitoring fibroblast behavior in tissue culture with an applied electric field," in *Proceedings of the National Academy of Sciences of the United States of America*, 1984, vol. 81, pp. 3761–3764.
- [5] C. R. Keese, K. Bhawe, J. Wegener, and I. Giaever, "Real-time impedance assay to follow the invasive activities of metastatic cells in culture," *BioTechniques*, vol. 33, no. 4, pp. 842–850, Oct. 2002, doi: 10.2144/02334rr01.
- [6] I. Giaever and C. R. Keese, "Use of electric fields to monitor the dynamical aspect of cell behavior in tissue culture," *IEEE Transactions on Biomedical Engineering*, vol. BME-33, no. 2, pp. 242–247, Feb. 1986, doi: 10.1109/TBME.1986.325896.
- [7] S. MacKay, P. Hermansen, D. Wishart, W. Hiebert, and J. Chen, "Simulating electrical properties of interdigitated electrode designs for impedance-based biosensing applications," in *2015 IEEE 28th Canadian Conference on Electrical and Computer Engineering (CCECE)*, May 2015, pp. 370–375, doi: 10.1109/CCECE.2015.7129305.
- [8] L. Q. Jun, G. W. bin Djaswadi, H. F. bin Hawari, and M. A. B Zakariya, "Simulation of interdigitated electrodes (IDEs) geometry using COMSOL multiphysics," in *2018 International Conference on Intelligent and Advanced System (ICIAS)*, Aug. 2018, pp. 1–6, doi: 10.1109/ICIAS.2018.8540599.
- [9] D. T. Price, A. R. A. Rahman, and S. Bhansali, "Design rule for optimization of microelectrodes used in electric cell-substrate impedance sensing (ECIS)," *Biosensors and Bioelectronics*, vol. 24, no. 7, pp. 2071–2076, Mar. 2009, doi: 10.1016/j.bios.2008.10.026.
- [10] G. Yang, H. Long, H. Tian, S. Luo, and H. Huang, "Bioimpedance measurement: modeling of coplanar electrodes and impedance characterization," in *2nd International Conference on Bioinformatics and Biomedical Engineering*, 2008, pp. 1248–1251, doi: 10.1109/ICBBE.2008.640.
- [11] F. Alexander, D. T. Price, and S. Bhansali, "Optimization of interdigitated electrode (IDE) arrays for impedance based evaluation of Hs 578T cancer cells," *Journal of Physics: Conference Series*, vol. 224, no. 1, Apr. 2010, doi: 10.1088/1742-6596/224/1/012134.
- [12] H. Bouyghf, B. Benhala, and A. Raihani, "Analysis of the impact of metal thickness and geometric parameters on the quality factor-Q in integrated spiral inductors by means of artificial bee colony technique," *International Journal of Electrical and Computer Engineering (IJECE)*, vol. 9, no. 4, pp. 2918–2931, Aug. 2019, doi: 10.11591/ijece.v9i4.pp2918-2931.
- [13] M. Ibrahim, J. Claudel, D. Kourtiche, and M. Nadi, "Geometric parameters optimization of planar interdigitated electrodes for bioimpedance spectroscopy," *Journal of Electrical Bioimpedance*, vol. 4, no. 1, pp. 13–22, Mar. 2013, doi: 10.5617/jeb.304.
- [14] X. Zhang, F. Li, K. Lee, and I. Voiculescu, "Lab-on-chip stretchable impedance spectroscopy device for mammalian cells studies," in *2017 19th International Conference on Solid-State Sensors, Actuators and Microsystems (TRANSDUCERS)*, Jun. 2017, pp. 1563–1566, doi: 10.1109/TRANSDUCERS.2017.7994359.
- [15] T. T. Ngo, A. Bourjilat, J. Claudel, D. Kourtiche, and M. Nadi, "Design and realization of a planar interdigital microsensor for biological medium characterization," *Smart Sensors, Measurement and Instrumentation*, vol. 16,




- pp. 23–54, 2016, doi: 10.1007/978-3-319-21671-3_2.
- [16] I. Sabiri, H. Bouyghf, and A. Raihani, “Optimal interdigitated electrode sensor design for biosensors using differential evolution algorithm,” in *E3S Web of Conferences*, May 2022, vol. 351, doi: 10.1051/e3sconf/202235101031.
- [17] W. Olthuis, W. Streekstra, and P. Bergveld, “Theoretical and experimental determination of cell constants of planar-interdigitated electrolyte conductivity sensors,” *Sensors and Actuators: B. Chemical*, vol. 24, no. 1–3, pp. 252–256, 1995, doi: 10.1016/0925-4005(95)85053-8.
- [18] V. Machairas, A. Tsangrassoulis, and K. Axarli, “Algorithms for optimization of building design: a review,” *Renewable and Sustainable Energy Reviews*, vol. 31, pp. 101–112, Mar. 2014, doi: 10.1016/j.rser.2013.11.036.
- [19] S. Sanaye and M. Dehghandokht, “Modeling and multi-objective optimization of parallel flow condenser using evolutionary algorithm,” *Applied Energy*, vol. 88, no. 5, pp. 1568–1577, 2011, doi: 10.1016/j.apenergy.2010.11.032.
- [20] G. D’Errico, T. Cerri, and G. Pertusi, “Multi-objective optimization of internal combustion engine by means of 1D fluid-dynamic models,” *Applied Energy*, vol. 88, no. 3, pp. 767–777, Mar. 2011, doi: 10.1016/j.apenergy.2010.09.001.
- [21] A. Mohammadi, M. Mohammadi, and S. H. Zahiri, “Design of optimal CMOS ring oscillator using an intelligent optimization tool,” *Soft Computing*, vol. 22, no. 24, pp. 8151–8166, 2018, doi: 10.1007/s00500-017-2759-4.
- [22] N. Delgarm, B. Sajadi, F. Kowsary, and S. Delgarm, “Multi-objective optimization of the building energy performance: A simulation-based approach by means of particle swarm optimization (PSO),” *Applied Energy*, vol. 170, pp. 293–303, May 2016, doi: 10.1016/j.apenergy.2016.02.141.
- [23] R. T. Marler and J. S. Arora, “Survey of multi-objective optimization methods for engineering,” *Structural and Multidisciplinary Optimization*, vol. 26, no. 6, pp. 369–395, 2004, doi: 10.1007/s00158-003-0368-6.
- [24] M. R.-Sierra and C. A. C. Coello, “Multi-objective particle swarm optimizers: a survey of the state-of-the-art,” *International Journal of Computational Intelligence Research*, vol. 2, no. 3, pp. 287–308, 2006.
- [25] A. Stoppato, G. Cavazzini, G. Ardizzone, and A. Rossetti, “A PSO (particle swarm optimization)-based model for the optimal management of a small PV (photovoltaic)-pump hydro energy storage in a rural dry area,” *Energy*, vol. 76, pp. 168–174, Nov. 2014, doi: 10.1016/j.energy.2014.06.004.
- [26] R. C. Eberhart and Y. Shi, “Tracking and optimizing dynamic systems with particle swarms,” in *Proceedings of the IEEE Conference on Evolutionary Computation*, 2001, vol. 1, pp. 94–100, doi: 10.1109/cec.2001.934376.

BIOGRAPHIES OF AUTHORS






Issa Sabiri    was born in Msemrir, Morocco on April 18, 1995. In 2016 he had got his license degree in Bio Medical Instrumentation and Maintenance, at the Institute of Health Sciences Settat-Morocco (ISSS) at the University Hassan I Settat-Morocco, then he had got a Master’s degree in biomedical engineering from FST Settat in 2018. He is currently a Ph.D. student in Laboratory of electrical engineering and intelligent systems (EEIS), ENSET Mohammedia, Hassan II University of Casablanca, Morocco. His works studies and interests are focused on development, design and optimization of electronic systems for biomedical engineering and health sciences. He can be contacted at email: issa.sabiri@etu.fstm.ac.ma.



Hamid Bouyghf    was born in Errachidia, Morocco in 1982. He received the B.S. and M.S. degrees in electrical engineering and telecom from the University of Science and Technology, Fez, Morocco, in 2007 and the Ph.D. degree in electrical engineering and telecom from Faculty of Science and Technic - Mohammedia, Hassan II University of Casablanca, Morocco, in 2019. From 2015 to 2019, he was a Research Assistant with the Princeton Plasma Physics Laboratory. Since 2019, he has been an Assistant Professor with the electrical Engineering Department, FST Mohammedia, Hassan II University, Casablanca, Morocco. He is the author of more articles in optimization of ICs area. His research interests include electronic applied to biomedical domain and analog ICs design, electromagnetic field, low power design, and BLE applications. He can be contacted at email: hamid.bouyghf@fstm.ac.ma.



Abdelhadi Raihani    was appointed as a professor in Electronics Engineering at Hassan II University of Casablanca, ENSET Institute, Mohammedia Morocco since 1991. He received the B.S. degree in Applied Electronics in 1991 from the ENSET Institute. He has his DEA diploma in Information Processing from Ben M’sik University of Casablanca in 1994. He received the Ph.D. in Parallel Architectures Application and Image Processing from the Ain Chock University of Casablanca in 1998. His current research interests are in the medical image processing areas, electrical engineering fields, particularly in renewable energy, energy management systems, power and energy systems control. He supervised several Ph.D. and Engineers students in these topics. He can be contacted at email: raihani@enset-media.ac.ma.